https://doi.org/10.5194/tc-2020-230
Preprint. Discussion started: 28 August 2020

The Cryosphere Discussions

Understanding Drivers of Glacier Length Variability Over the Last Millennium

Alan Huston[1], Nicholas Siler[1], Gerard H. Roe[2], Erin Pettit[1], and Nathan J. Steiger[3,4]

[1]College of Earth, Ocean, and Atmospheric Sciences, Oregon State University, Corvallis, OR, USA
[2]Department of Earth and Space Sciences, University of Washington, Seattle, WA, USA
[3]Institute of Earth Sciences, Hebrew University, Jerusalem, Israel
[4]Lamont-Doherty Earth Observatory, Columbia University, Palisades, NY, USA

Correspondence: Nicholas Siler (nick.siler@oregonstate.edu)

Abstract. Changes in glacier length reflect the integrated response to local fluctuations in temperature and precipitation resulting from both external forcing (e.g., volcanic eruptions or anthropogenic CO_2) and internal climate variability. In order to interpret the climate history reflected in the glacier moraine record, therefore, the influence of both sources of climate variability must be considered. Here we study the last millennium of glacier length variability across the globe using a simple dynamic glacier model, which we force with temperature and precipitation time series from a 13-member ensemble of simulations from a global climate model. The ensemble allows us to quantify the contributions to glacier length variability from external forcing (given by the ensemble mean) and internal variability (given by the ensemble spread). Within this framework, we find that internal variability drives most length changes in mountain glaciers that have a response timescale of less than a few decades. However, for glaciers with longer response timescales (more than a few decades) external forcing has a greater influence than internal variability. We further find that external forcing also dominates when the response of glaciers from widely separated regions is averaged. Single-forcing simulations indicate that most of the forced response over the last millennium, pre-anthropogenic warming, has been driven by global-scale temperature change associated with volcanic aerosols.

1 Introduction

The length of a glacier reflects both its topographic and climate setting, and arises from a balance between accumulation (mass gain) and ablation (mass loss), mediated by the catchment geometry and the dynamics of ice flow. Past fluctuations in glacier length often leave moraines on the landscape. If the age of these moraines can be determined, they become valuable proxies of past climate change (e.g., Solomina et al., 2015). The decadal-and-longer response time of glacier length means that glaciers act as low-pass filters of climate, and thereby have the potential to reveal climate trends that would otherwise go undetected (Balco, 2009).

Changes in climate can arise from three factors: first, the internal climate variability that would occur in the atmosphere-ocean-cryosphere system even under constant external conditions; second, natural climate forcings, such as solar luminosity, variations in the Earth's orbit, and volcanic eruptions that act to change the Earth's energy budget; and third, anthropogenic forcing, such as emissions of CO_2 and industrial aerosols.

https://doi.org/10.5194/tc-2020-230
Preprint. Discussion started: 28 August 2020


The Cryosphere Discussions

Until recently, variations in glacier length over the pre-industrial Holocene have mostly been attributed to natural forcing of climate. For example, Crowley (2000) estimated that 40-to-65 % of pre-anthropogenic decadal-scale temperature variations were a result of changes in solar irradiance and volcanism. Similarly, Miller et al. (2012) have argued that the Little Ice Age period between approximately 1300 and 1850 was caused by a sequence of volcanic eruptions, with the cooling effects of explosive volcanism made more persistent by sea-ice/ocean feedbacks operating long after the volcanic aerosols were removed from the atmosphere.

However, recent studies have shown that large variability in glacier length can also occur in an unforced, statistically constant climate due to internal climate variability (e.g., Oerlemans, 2000). By studying glaciers around Mt. Baker in Washington State, for example, Roe and O'Neal (2009) found that internal variability alone can produce kilometer-scale excursions in glacier length on multi-decadal and centennial timescales. This result highlights the importance of considering internal variability in addition to forced climate change as a potential cause of past variations in glacier length. Until now, however, no systematic assessment of the relative importance of forced versus internal variability has been conducted.

Both the local magnitude and the spatial coherence of glacier length variability have been studied for specific regions using existing observations. For example, there is a notable inter-hemispheric disparity in the timing of the maximum ice extent during the Holocene for glaciers in New Zealand versus the Alps (Schaefer et al., 2009). Additionally, mid-to-late Holocene glacier fluctuations were neither in phase nor in strict anti-phase between the hemispheres, suggesting that regional climate variability has played an important role (Schaefer et al., 2009). Indeed, the very idea of a global-scale Little Ice Age or Medieval Climate Anomaly has been called into question (Neukom et al., 2019).

Here we use an ensemble of simulations of a global climate model and a simple dynamical glacier model to evaluate the magnitude and spatial coherence of the glacier response worldwide. These results provide a quantitative framework for interpreting the geologic record of glacier change, as well as for how glaciers are likely to respond to anthropogenic warming in coming decades.

2 Quantifying forced and internal climate variability over the last millennium

We analyze simulated climate variability within the Community Earth System Model (CESM) Last Millennium Ensemble (LME). The LME comprises 13 simulations that span 850-2005 CE (Otto-Bliesner et al., 2016). Each simulation includes the same radiative forcing contributions from volcanic aerosols, solar irradiance, orbital changes, greenhouse gases, and ozone aerosols, based on forcing reconstructions from the fifth-generation Coupled Model Intercomparison Project (CMIP5; Schmidt et al., 2011). The ensemble members all have exactly the same physics, and differ only in their initial conditions. Chaotic internal dynamics and the different initial conditions cause a spread among the ensemble members. The ensemble mean captures most of the forced climate response, while the ensemble spread represents internal climate variability.

Our focus is on glaciers, so we present our analysis of climate variability in terms of the factors relevant for mass balance (net accumulation or ablation) at real-world glaciers. First, we identify the grid points in the CESM model that are closest to glaciers for which the inter-annual variability in summer and winter mass balance is known (Medwedeff and Roe, 2017, and Table A1).

https://doi.org/10.5194/tc-2020-230
Preprint. Discussion started: 28 August 2020


The Cryosphere Discussions
Open Access
EGU

At each of these grid points, we compute annual time series of average winter precipitation (P) and summer temperature (T). For grid points in the Northern Hemisphere, P is taken from October-March and T is taken from April-September. The seasons are flipped for grid points in the Southern Hemisphere. We then estimate mass-balance variability using the following linear approximations,

$$b'_w = \alpha P' \tag{1}$$

$$b'_s = -\lambda T', \tag{2}$$

where b_w and b_s represent winter and summer mass balance, α and λ are positive constants, and primes indicate anomalies relative to the millennial average (1000-1999). Note that the negative sign in Eq. 2 reflects an anticorrelation between mass balance and temperature in the summer.

Like most GCMs, the grid resolution of the LME is too coarse to capture the full influence of orography on P and T at most glacier locations. To compensate for this, we choose values of α and λ for each glacier that produce variances in b'_w and b'_s that match the observed values reported by Medwedeff and Roe (2017). This is achieved by setting

$$\alpha = \frac{\sigma_{b,w}}{\sigma_P} \tag{3}$$

$$\lambda = \frac{\sigma_{b,s}}{\sigma_T}, \tag{4}$$

where the numerators represent the observed standard deviations in winter and summer mass balance, and the denominators represent the standard deviations in winter precipitation and summer temperature. Annual mass-balance anomalies are then given by

$$b' = b'_w + b'_s. \tag{5}$$

For this portion of our analysis, we focus on three geographically diverse glaciers: i) the Silvretta glacier in the Alps, ii) the South Cascade glacier in the American Pacific Northwest, and iii) the Martial Este glacier in the Patagonian Andes. Figure 1 shows the time series of winter mass-balance anomalies (b'_w; Fig. 1a), summer mass-balance anomalies (b'_s; Fig. 1b), and annual mass-balance anomalies (b'; Fig. 1c) at these three glaciers, with their average shown in green at the bottom of each panel. The heavy colors indicate the ensemble-mean anomalies, while the lighter colors represent the range of ensemble members. The vertical grey line at the year 1880 marks the approximate transition from the pre-industrial era to the modern era, after which the time axis on each panel is dilated by a factor of 4 to enhance visibility. We evaluate the accuracy of LME temperatures over the modern era by plotting values of b'_s calculated from observed temperature anomalies (NASA GISS dataset; Lenssen et al., 2019) using Eq. 2 (Fig. 1b, black lines).

https://doi.org/10.5194/tc-2020-230
Preprint. Discussion started: 28 August 2020

The ensemble mean mostly represents the response to external forcing. The importance of this forcing relative to the internal variability can be measured by a signal-to-noise ratio (SNR), which we define as

$$\mathrm{SNR} = \frac{\mathrm{Var}[\overline{b'}(t)]}{\mathrm{Var}[b'(t)] - \mathrm{Var}[\overline{b'}(t)]}, \tag{6}$$

where $\mathrm{Var}[\overline{b'}(t)]$ is the variance of the ensemble mean time series (i.e., an approximation of the forced response, or "signal"), and $\mathrm{Var}[b'(t)]$ is the total variance across all ensemble members. The difference between these two quantities in the denominator represents the variance due to internal climate variability (i.e., the "noise"). In general, SNR values less than one indicate that most of the variance in a time series can be attributed to internal variability, while SNR values greater than one indicate that most variance is driven by external forcing. For a 13-member ensemble, SNR values greater than 0.125 in the modern era or 0.098 in the pre-industrial era indicate that a forced signal can be detected and is statistically significant at the 99% confidence level (see Appendix). SNR values are listed in Fig. 1 for each time series and time period, with bold font indicating statistical significance.

In the winter (Fig. 1a), there is little evidence of a forced signal in b'_w at any glacier during either time period, as indicated by SNR values that are uniformly low and statistically insignificant. This implies that interannual variability in winter mass balance (and thus winter precipitation) at these glaciers is dominated by internal climate noise. This finding is expected based on past studies of the contribution from winter precipitation trends in glacier change (e.g., Medwedeff and Roe, 2017).

In contrast, b'_s shows clear evidence of a forced signal (Fig. 1b). During the pre-industrial period, all locations exhibit several abrupt spikes associated with volcanic eruptions, with the most notable event being the Samalas eruption in 1257 (e.g., Guillet et al., 2017). The amplitude of these spikes is strongest in Europe and North America, where they occur against the backdrop of a longer-term increase in b'_s associated with a cooling trend that persists through the end of the 19th century. Although the forced signal is statistically significant at all locations during the pre-industrial period, SNR values are less than 0.2, implying that internal noise still accounts for the majority of local year-to-year temperature variability.

Around 1900, b'_s begins to decrease at all three glaciers in response to global warming (Fig. 1b). SNR values are greater in this period than in the pre-industrial period, reflecting the unprecedented strength and persistence of anthropogenic forcing. Comparing the simulated trends in b'_s over the 20th century with those derived from observed temperatures (Fig. 1b; colored vs. black lines), we find good agreement at South Cascade and Martial Este but not at Silvretta, where the decrease in b'_s in the LME ensemble mean is too low by 0.07 m/decade, reflecting a warming trend that is too low by 0.063 K/decade (Eq. 2, with $\lambda = 1.11$ m K^{-1}). One possible interpretation of this difference is that part of the observed warming trend at Silvretta was the result of internal variability. This conclusion is supported by the fact that the observed trend at Silvretta lies within the ensemble range of simulated trends. On the other hand, 20th-century warming trends in the LME are weaker than observed trends over most of the globe (Fig. A1), suggesting that model bias likely also plays a role. We consider possible causes of this bias in Section 3.4, but note that it does not affect the bulk of our analysis.

Finally, variability in b' (Fig. 1c) shows the influence of both b'_w and b'_s, but in different proportions for each glacier. For example, at South Cascade glacier (red), the variance in b'_w is a factor of 2 greater than the variance in b'_s, and thus exerts a much stronger influence on b'. Because b'_w is essentially noise, the SNR of b' at South Cascade glacier is statistically insignificant

https://doi.org/10.5194/tc-2020-230
Preprint. Discussion started: 28 August 2020


The Cryosphere Discussions
Open Access
EGU

in the modern era, even though b'_s contains a significant forced signal. This masking of forced variance in b' by large internal variance in b'_w despite the presence of forced variance in b'_s is typical of maritime glaciers and detailed, for example, in Young et al. (2020). At Silvretta and Martial Este, by contrast, the variance comes mostly from b'_s. Thus, while b'_w remains a source of noise, its amplitude is small enough that the forced signal from b'_s can still be detected in b'.

A final point to emphasize from Fig. 1 relates to the averaged time series among the three glaciers (green lines). These exhibit higher SNRs in b'_s and b' than any individual glacier, suggesting that spatial averaging may help suppress noise and bring out a common forced signal. This echoes results from studies of modern-day warming, which have found that the anthropogenic signal is clearest at global scales, even when it is obscured by internal variability at local and regional scales (e.g., Deser et al., 2012). We elaborate on the reasons for this result in Section 3.2 below.

3 Glacier simulations

To simulate variability in glacier length, we use the three-stage linear model of Roe and Baker (2014), which has been shown to better capture the high-frequency response of glacier dynamics than earlier low-order models (Harrison and Post, 2003; Oerlemans, 2000, 2005). The three stages, which can be diagnosed from ice dynamics in numerical models, are: (1) changes in interior thickness, which drive (2) changes in terminus ice flux, which in turn drive (3) changes in glacier length. Collectively, the three stages can be represented as a linear, third-order differential equation,

$$\left(\frac{d}{dt}+\frac{1}{\epsilon\tau}\right)^3 L' = \frac{1}{\epsilon(\epsilon\tau)^2}\beta b', \tag{7}$$

where L' is the length anomaly as a function of time, t; b' is the annual mass balance anomaly derived from LME output; ϵ is the ratio of the variances in the three-stage and one-stage models, which is set to $1/\sqrt{3}$; τ is the glacier response timescale, and β is a non-dimensional shape parameter that only affects the amplitude of L', and not its temporal characteristics. The glacier response time is given by $\tau = -H/b_t$, where H is a characteristic ice thickness in the terminus zone and b_t is the net (negative) mass balance in the terminus zone (Jóhannesson et al., 1989). Note there is not necessarily a simple relationship between τ and glacier size: cirque glaciers can be thick and have termini that extend only a little past the equilibrium line altitude, giving them τs of many decades (e.g., Barth et al., 2017). Conversely, glaciers sourced from large accumulation areas may have termini well below the equilibrium line altitude, and if terminating on steep slopes, also be relatively thin, giving them short τs of a decade or less (e.g., Franz Joseph N.Z., Purdie et al., 2014).

The three-stage model accurately emulates the autocorrelation function and power spectrum of numerical flowline models of ice dynamics (Christian et al., 2018; Roe and Baker, 2014) and has been shown to produce realistic length responses to climate trends and variability given appropriate choices of τ and β (e.g., Herla et al., 2017).

In the simulations we present here, we did not attempt to assign realistic values of τ and β to each glacier. Rather, for each glacier, we performed three separate simulations with $\tau = 10$, 30, and 100 years, and $\beta = 150$. This approach has two main advantages. First, the subset of glaciers analyzed in Fig. 1 are located in regions with a wide range of glacier sizes. Simulating a range of response timescales thus gives a more complete picture of glacier variability in these regions. Second, it

https://doi.org/10.5194/tc-2020-230
Preprint. Discussion started: 28 August 2020

allows us to perform a controlled test of how SNR varies with response timescale, which we will demonstrate has important implications for how geologic records of past glacier variability ought to be best interpreted. This range of τ encompasses most alpine glaciers (e.g., Haeberli and Hoelzle, 1995; Lüthi et al., 2010; Roe et al., 2017). The value of β is a function of glacier geometry: $\beta = A/wH$, where A is the surface area, and w and H are the characteristic width and thickness of the glacier in the terminus zone. Our choice of $\beta = 150$ is based on Hintereisferner in the Austrian Alps ($A = 10$ km^2, $w = 400$ m, $H = 170$ m, Herla et al., 2017). The equation for L' is linear, and so the value of β does not affect the relative importance of different kinds of climate forcing.

Figure 2 shows the glacier length anomalies (L') that result from the time series of b' shown in Fig. 1c. The columns of Fig. 2 correspond to response timescales of $\tau = 10$ years (left), 30 years (middle), and 100 years (right). In each panel, the heavy line represents the ensemble mean, while the light colors represent each of the 13 ensemble members. SNR values were computed using the same method described in Section 2, and are shown in the bottom right of each panel for the pre-industrial era alone (1000-1880), to avoid the distorting effects of more recent anthropogenic warming. The magnitude of the fluctuations is somewhat arbitrary and will change with catchment geometry.

Comparing the columns of Fig. 2, we find that the time series of L' become increasingly smooth as τ increases, indicating a progressive “reddening" of the variance spectra. This reflects the fact that glaciers essentially act as low-pass filters of annual mass balance. The spectral power drops sharply at frequencies higher than $1/(2\pi\tau)$ (Roe and Baker, 2014). During the pre-industrial period, positive trends in L' across the Northern Hemisphere reflect a cooling trend within the LME, as noted previously (Fig. 1b). Conversely, during the past century of anthropogenic warming, negative trends in L' are found at all locations when $\tau = 10$ years, but only in the Southern Hemisphere when $\tau = 100$ years. The absence of 20th-century retreat in the Northern Hemisphere partially reflects the muted warming trend in the LME relative to observations (Fig. A1). However, the difference in recent trends between $\tau = 10$ years and $\tau = 30$ years also illustrates a more general point: namely, that higher τ values imply a more delayed response to a given climate perturbation. We discuss the implications of this result for future changes in glacier length in Section 4.

In addition to the ensemble-mean differences discussed above, the panels in Fig. 2 also exhibit significant differences in ensemble spread. These differences are most clearly illustrated by SNR values, which reveal two key dependencies. First, at all locations, SNR increases monotonically with increasing timescale (i.e., from left to right in Fig. 2). Notably, we find a similar increase in SNR with τ at all other glacier locations as well (Fig. A2), suggesting that it reflects a general property of the climate system. Large-τ glaciers are usually more reliable indicators of forced climate change than small-τ glaciers, which are more prone to natural fluctuations. There is a trade-off: the larger-τ glaciers smooth over longer periods and so the temporal resolution of the forced change is degraded.

Second, SNR is substantially greater in the spatially-averaged time series of glacier length (Fig. 2, bottom row) than it is for any individual glacier, similar to what we found with annual mass balance (Fig. 1). This suggests that glacier variability is more likely to reflect external forcing if the glacier variability is coherent across a large spatial domain. We address each of these behaviors in greater detail below. We also extend our analysis to a larger set of 76 glaciers, for which variability in summer and winter mass balance were also provided by Medwedeff and Roe (2017, Table A1).

https://doi.org/10.5194/tc-2020-230
Preprint. Discussion started: 28 August 2020

3.1 Dependence of SNR on timescale

The relationship between SNR and τ evident in Fig. 2 stems from differences in how natural and forced variance is distributed across the frequency spectrum. These differences are illustrated in Fig. 3, which shows the spectra of unforced and forced annual mass balance (b) variability in the top row, with subsequent rows showing equivalent results for winter precipitation (P) and summer temperature (T). Gray lines represent the spectra at the locations of all 76 glaciers in our data set, while colored lines represent the subset of three glaciers analyzed in Figs. 1 and 2. As in those figures, the green line represents the spectrum of the average time series across the three glaciers, while the black line represents the average of all individual spectra across the 76 glaciers. Average slopes of the various spectra were calculated using linear regression, and are shown in the bottom left of each panel.

Comparing the spectra of unforced and forced mass-balance variability in the top row of Fig. 3, we find that the unforced spectrum is essentially white (i.e., it has a flat spectral slope), while the forced spectrum is red, exhibiting greater variance at low frequencies. Therefore, when low-pass filtered by the glacier response, more of the forced variability is retained by the glacier, resulting in higher SNR values in glacier length relative to annual mass balance. This effect becomes larger as τ increases and the filter cutoff shifts to lower frequencies, thus explaining the positive correlation between SNR and τ found in Fig. 2.

The source of the differences in slope between the forced and unforced mass-balance spectra is evident in Fig. 3c-f, which show the same spectral decompositions for P and T. The spectra of P are essentially flat at all frequencies, indicative of white noise generated by internal atmospheric variability (Fig. 3c-d). This is equally true of the forced and unforced components, providing further evidence that most of the “signal" in ensemble-mean precipitation is not physical, but rather residual noise retained during the averaging (Fig. 1). Similarly, the unforced T spectra (Fig. 3e) are also mostly white, except at the highest frequencies where variance is likely damped by interannual persistence in sea surface temperatures. In contrast, the forced T spectra are significantly red at all frequencies (Fig. 3f), and are thus clearly responsible for the similar slopes of the forced mass balance spectra (Fig. 3b).

The redness of the forced mass-balance spectra in Fig. 3b is not evident in the spectrum of volcanic forcing, which is white at sub-decadal frequencies (Fig. A3). It must therefore be caused by reddening mechanisms inherent to the climate system, such as ocean heat storage and sea-ice feedbacks (Stenchikov et al., 2009; Miller et al., 2012). GCM simulations have further shown that strong, abrupt forcing from volcanic aerosols can also be reddened by enhanced heat exchange with the deep ocean, due to a strengthening of both vertical mixing and the Atlantic Meridional Overturning Circulation (AMOC) (Stenchikov et al., 2009). This unique response to volcanic forcing may help explain why the forced spectra of T and b are so much redder than the unforced spectra (Fig. 3). However, further research is needed to fully understand the difference in spectral slopes between forced and internal temperature variability.

https://doi.org/10.5194/tc-2020-230
Preprint. Discussion started: 28 August 2020

3.2 Dependence of SNR on spatial scale

We now compare the spatial coherence of the forced and unforced responses among the set of 76 glaciers. The top row of Fig. 4 shows the simultaneous cross-correlation matrices for the time series of unforced and forced glacier length. The correlations were computed assuming $\tau = 10$ years for each glacier, but the results are similar for $\tau = 30$ and 100 years (not shown). For natural variability (Fig. 4a), we find strong correlations at the scale of individual mountain ranges, but not at larger scales. For example, while all glaciers in the Alps are strongly correlated with each other, they are not significantly correlated with glaciers in Scandinavia. This implies that internal variability has a relatively short decorrelation scale, consistent with synoptic-scale atmospheric variability (e.g., Wallace and Hobbs, 2006). By contrast, cross-correlations among the forced time series of glacier length are significantly positive among a large majority of glacier pairs (92%; Fig. 4b), indicating that climate changes resulting from external forcing are globally coherent (Fig. 4b). When multiple time series of glacier length are averaged across different mountain ranges, the incoherent internal noise is damped relative to the coherent forced signal. This explains why the SNR of the averaged time series of glacier length is greater than the SNR at any individual glacier (Fig. 2).

The bottom two rows of Fig. 4 show the same cross-correlation matrices as in the top row, but with glacier length time series separated into contributions from T and P. In the unforced case (Figs. 3c,e), the correlation patterns resulting from both T- and P-driven length variability resemble the total unforced correlations in Fig. 3a. One exception is in the P-driven matrix (Fig. 3c), where negative correlations indicate the existence of dipole patterns between adjacent regions, such as the Alps and Scandinavia, or the Pacific Northwest and Alaska. However, these dipole patterns have a relatively small impact on the total unforced correlations across these regions. Meanwhile, the decomposition of the forced correlations (Figs. 4d,f) shows that the global coherence of forced glacier variability comes entirely from T rather than P. Precipitation-driven variability is a source of noise that mostly weakens the correlations, but does not change their global coherence.

3.3 The relative importance of precipitation versus temperature

The preceding analysis has shown that forced changes in glacier length are driven primarily by globally-coherent changes in summer temperature. However, this result provides little insight into the relative importance of temperature versus precipitation in driving glacier variability more generally. These contributions are quantified in Fig. 5, which shows the ratio of T-driven variance to total variance, both in annual mass balance (Fig. 5a), and in glacier length (Fig. 5b; assuming $\tau = 10$ years). Because T and P are not significantly correlated at any glacier location, this ratio approximately represents the fraction of total variance that can be attributed to T. The difference between the two panels is shown in Fig. 5c.

In the case of annual mass balance, T accounts for more than half the variance at 58 out of 76 glaciers, with an average value of 67% of the total variance among all glaciers. The few glaciers where precipitation variability plays a larger role are mostly located in maritime environments with large storm-track variability, such as Alaska, the Pacific Northwest, and the Andes. In contrast, variability in glacier length is dominated by temperature everywhere (Fig. 5b), including at glaciers (like South Cascade) where precipitation accounts for most of the variability in annual mass balance.

https://doi.org/10.5194/tc-2020-230
Preprint. Discussion started: 28 August 2020

Why does temperature exert a greater influence on glacier length than on annual mass balance? Recall from Fig. 3 that the spectrum of T is redder than the spectrum of P. This difference is especially pronounced in the forced time series, but it is also evident in the unforced time series at frequencies greater than $\sim$ 1/decade, where T variance is suppressed by SST persistence. As low-pass filters, glaciers eliminate variance at the highest frequencies, where precipitation's contribution to annual mass balance variance is greatest. Thus, for the same reasons that SNR is enhanced by a glacier's filtering properties, the contribution of temperature to glacier-length variability is enhanced relative to that of precipitation. This means that fluctuations in glacier-length variability primarily reflect low-frequency variability in summer temperature, even where mass-balance variability is more strongly influenced by winter precipitation.

3.4 Roles of individual forcings

Finally, we evaluate the relative importance of the different climate-forcing factors in these simulations. In addition to the full 13-member ensemble, the LME archive also contains smaller ensembles of simulations representing the climate response to single factors. The factors (and the number of ensemble members) are: greenhouse gases (3), volcanic aerosols (5), industrial aerosols (5), and changes in solar and orbital patterns (3). As in the full-forcing ensemble, we use the ensemble mean to approximate the climate response to each individual factor. However, it is important to note that these approximations contain substantially more noise than the full ensemble mean because there are fewer ensemble members.

Figure 6 shows the time series of glacier length anomalies induced by each individual forcing factor, averaged among all ensemble members and all glaciers in the Northern Hemisphere (top) and Southern Hemisphere (bottom). Results are presented for $\tau = 10$ years and $\tau = 30$ years. The contributions from the solar and orbital forcing were negligible and are not shown.

During the pre-industrial era, most of the forced variability in glacier length can be attributed to volcanic aerosols (Fig. 6, red and green lines). Over the last century, however, anthropogenic factors have played the largest role. In the Southern Hemisphere, the full-forcing time series closely follows greenhouse-gas-driven trends beginning around the year 1850. In the Northern Hemisphere, by contrast, retreat due to greenhouse gases is largely offset by industrial aerosol emissions during the modern era. While it is well known that industrial aerosols provided radiative cooling over the 20th century, warming trends over this period are generally lower in the LME than in observations (Fig. A1), suggesting that the model's aerosol forcing may be too strong, or that its transient climate sensitivity may be too low. Whatever the cause, the suppressed 20th-century warming trend in many regions within the LME explains why our simulations appear to show less glacier retreat than has been observed in some locations (e.g., Herla et al., 2017).

4 Summary and Discussion

In this study, we have combined an ensemble of numerical climate model simulations and a glacier length model to evaluate the relative importance of climate forcing and internal climate variability in driving glacier-length fluctuations. While the potential importance of internal variability has been noted before, this is the first study to evaluate the relative importance of natural forcing vs. internal variability in the pre-industrial era, and the accompanying spatial patterns of glacier response. We

https://doi.org/10.5194/tc-2020-230
Preprint. Discussion started: 28 August 2020

estimated annual mass balance anomalies over the last millennium at 76 glaciers around the world using simulated time series of summer temperature and winter precipitation from the 13-member CESM Last Millennium Ensemble. Using the three-stage linear model of Roe and Baker (2014), we then converted these mass-balance anomalies into glacier-length anomalies for a range of glacier response timescales, thus capturing the diversity of behavior exhibited by glaciers of different sizes and geometries. Because the ensemble simulations differ only in their initial conditions, the responses of mass balance and glacier length to external radiative forcing are mostly captured by the ensemble mean, while internal unforced variability is represented by departures from the ensemble mean (i.e., the ensemble spread). The ratio of ensemble-mean variance to ensemble-spread variance is defined as the signal-to-noise ratio (SNR), and represents the fraction of total variance driven by external forcing.

While SNR varies by location, we found that two factors influence SNR more generally. First, SNR is greater for glacier length than for annual mass balance, and increases further with increasing glacier response timescale, τ. This timescale-dependence reflects differences in how forced and unforced mass-balance variance is distributed across the frequency spectrum. Specifically, because forced variance has a redder spectrum than unforced variance, the forced signal is amplified relative to unforced noise when low-pass-filtered by a glacier. This explains why a glacier like South Cascade, which does not exhibit a significant forced response in annual mass balance due to high interannual variability (Fig. 1, red), still shows a significant forced response in glacier length in our simulations (Fig. 2, red).

For both mass balance and glacier length, SNR is enhanced by averaging multiple time series from different locations. This is because forced changes in mass balance tend to be globally coherent, reflecting a global-scale temperature response, while unforced variability has little coherence beyond the scale of an individual mountain range.

Our results have implications for how past glacier variability should be interpreted. For example, because SNR increases with spatial averaging, a change in glacier length is more likely to be forced when coherent changes are also observed in other mountain ranges.

However, it is important to recognize that the amplified signal in large-τ glaciers comes at the expense of decreased temporal resolution. Thus, while large-τ glaciers may be more reliable indicators of climate change on centennial timescales, they may entirely miss climate changes that occur on multi-decadal timescales.

Differences in response time also have implications for how glaciers have responded and will respond to global warming. Because glaciers are lagging indicators of climate change, recent glacier retreat has been more modest than the decrease in annual mass balance (Figs. 1 and 2), implying that further retreat is locked in, even in the absence of additional warming (Christian et al., 2018). This disequilibrium is especially pronounced for large-τ glaciers, whose slow response means that they have only begun to feel the effects of the past century of warming. In future decades, therefore, we expect that large-τ glaciers will experience the greatest retreat, as they integrate the effects of both past and future warming.

Our analyses have been made possible by ensemble climate modeling. As done here, such ensembles can be used to decompose the contributions due to internal variability and natural and anthropogenic forcing. However, we have used only one climate model. As other ensembles become more widely available it will be important to evaluate different climate models, and also different estimates of the natural and anthropogenic forcing, for which there are still significant uncertainties (Schmidt et al., 2011). Lastly, we have analyzed continuous time series of glacier length. Actual records of past glacier extent are more

https://doi.org/10.5194/tc-2020-230
Preprint. Discussion started: 28 August 2020

fragmentary, with moraines representing periods of maximum extent that were not subsequently over-ridden by a later advance. An interesting extension of this study would be to make estimates of the moraine record that might be left on the landscape.

Data availability. Output from the CESM Last Millennium Ensemble can be downloaded from the National Center for Atmospheric Research (NCAR) Climate Data Gateway: https://www.earthsystemgrid.org/.

Appendix A: Statistical significance of SNR

We consider a signal-to-noise ratio (SNR) to be statistically significant if we can reject the null hypothesis that $\mathrm{SNR} = 0$ with at least 99% confidence ($p < 0.01$). To determine the threshold for statistical significance, we performed a Monte Carlo simulation consisting of 100,000 ensembles of 13 randomly generated Gaussian time series (i.e., noise). We set the length of each synthetic time series based on the estimated degrees of freedom in the given climate variable, as described below. For each 13-member ensemble, we compute the SNR as in Eq. 6. This yields a set of 100,000 synthetic SNR values which have a mean of 0.083 and a distribution that depends on the number of degrees of freedom in the time series. Because the true SNR of each ensemble is equal to 0, we set the threshold for statistical significance to be the 99th percentile of SNR values within the distribution.

At all glacier locations within the LME, we find that time series of winter precipitation and summer temperature exhibit an e-folding decorrelation scale of no more than 1 year. Thus, for time series of summer and winter mass balance, we assume the number of degrees of freedom is equal to half the number of years in the stated time period Leith (1973). This yields significance thresholds of 0.098 for the pre-industrial and 0.125 for the modern.

For the glacier length time series, we find that the e-folding decorrelation scale is on average equal to about 1.5τ. Over the pre-industrial period, this implies about 30, 10, and 3 degrees of freedom for $\tau = 10$, 30, and 100 years, respectively. The corresponding SNR significance thresholds are found to be 0.15 for $\tau = 10$ years, 0.22 for $\tau = 30$ years, and 0.49 for $\tau = 100$ years. All of our simulated glacier length time series have SNR values that exceed these thresholds.

Author contributions. Huston and Siler performed the analysis and wrote the paper. Roe and Siler designed the study. All authors helped interpret the results and edit the paper.

Competing interests. The authors have no competing interests.

https://doi.org/10.5194/tc-2020-230
Preprint. Discussion started: 28 August 2020

Acknowledgements. We thank John Fasullo for providing time series of individual forcing agents used in the LME. We thank the Oregon State University Honors College for supporting this research. This work was funded by the US National Science Foundation grants AGS-2024212, AGS-1805490, AGS-1903465. LDEO contribution number XXXX.

https://doi.org/10.5194/tc-2020-230
Preprint. Discussion started: 28 August 2020

References

Balco, G.: The Geographic Footprint of Glacier Change, Science, 324, 599–600, https://doi.org/10.1126/science.1172468, 2009.

Christian, J. E., Koutnik, M., and Roe, G.: Committed retreat: controls on glacier disequilibrium in a warming climate, Journal of Glaciology, 64, 675–688, https://doi.org/10.1017/jog.2018.57, 2018.

Crowley, T. J.: Causes of climate change over the past 1000 years, Science, 289, 270–277, https://doi.org/10.1126/science.289.5477.270, 2000.

Deser, C., Phillips, A., Bourdette, V., and Teng, H.: Uncertainty in climate change projections: The role of internal variability, Climate Dynamics, 38, 527–546, https://doi.org/10.1007/s00382-010-0977-x, 2012.

Guillet, S., Corona, C., Stoffel, M., Khodri, M., Lavigne, F., Ortega, P., Eckert, N., Sielenou, P. D., Daux, V., Churakova Sidorova, O. V., Davi, N., Edouard, J. L., Zhang, Y., Luckman, B. H., Myglan, V. S., Guiot, J., Beniston, M., Masson-Delmotte, V., and Oppenheimer, C.: Climate response to the Samalas volcanic eruption in 1257 revealed by proxy records, Nature Geoscience, 10, 123–128, https://doi.org/10.1038/ngeo2875, 2017.

Harrison, W. D. and Post, A. S.: How much do we really know about glacier surging?, Annals of Glaciology, 36, 1–6, https://doi.org/10.3189/172756403781816185, 2003.

Herla, F., Roe, G. H., and Marzeion, B.: Ensemble statistics of a geometric glacier length model, Annals of Glaciology, 58, 130–135, https://doi.org/10.1017/aog.2017.15, 2017.

Jóhannesson, T., Raymond, C., and Waddington, E.: Time–Scale for Adjustment of Glaciers to Changes in Mass Balance, Journal of Glaciology, 35, 355–369, https://doi.org/10.3189/S002214300000928X, 1989.

Leith, C.: The Standard Error of Time-Average Estimates of Climatic Means, Journal of Applied Meteorology and Climatology, 12, 1066–1069, https://doi.org/10.1175/1520-0450(1973)012%3C1066:TSEOTA%3E2.0.CO;2, 1973.

Lenssen, N., Schmidt, G., Hansen, J., Menne, M., Persin, A., Ruedy, R., and Zyss, D.: Improvements in the GISTEMP uncertainty model, J. Geophys. Res. Atmos., 124, 6307–6326, https://doi.org/10.1029/2018JD029522, 2019.

Medwedeff, W. G. and Roe, G. H.: Trends and variability in the global dataset of glacier mass balance, Climate Dynamics, 48, 3085–3097, https://doi.org/10.1007/s00382-016-3253-x, 2017.

Miller, G. H., Geirsdóttir, Á., Zhong, Y., Larsen, D. J., Otto-Bliesner, B. L., Holland, M. M., Bailey, D. A., Refsnider, K. A., Lehman, S. J., Southon, J. R., Anderson, C., Björnsson, H., and Thordarson, T.: Abrupt onset of the Little Ice Age triggered by volcanism and sustained by sea-ice/ocean feedbacks, Geophysical Research Letters, 39, 1–5, https://doi.org/10.1029/2011GL050168, 2012.

Neukom, R., Steiger, N., Gómez-Navarro, J. J., Wang, J., and Werner, J. P.: No evidence for globally coherent warm and cold periods over the preindustrial Common Era, Nature, 571, 550–554, https://doi.org/10.1038/s41586-019-1401-2, https://doi.org/10.1038/s41586-019-1401-2, 2019.

Oerlemans, J.: Holocene glacier fluctuations: Is the current of retreat exceptional?, Annals of Glaciology, 31, 39–44, https://doi.org/10.3189/172756400781820246, 2000.

Oerlemans, J.: Extracting a climate signal from 169 glacier records, Science, 308, 675–677, https://doi.org/10.1126/science.1107046, 2005.

Otto-Bliesner, B. L., Brady, E. C., Fasullo, J., Jahn, A., Landrum, L., Stevenson, S., Rosenbloom, N., Mai, A., and Strand, G.: Climate variability and change since 850 ce an ensemble approach with the community earth system model, Bulletin of the American Meteorological Society, 97, 787–801, https://doi.org/10.1175/BAMS-D-14-00233.1, 2016.

https://doi.org/10.5194/tc-2020-230
Preprint. Discussion started: 28 August 2020

Purdie, H., Anderson, B., Chinn, T., Owens, I., Mackintosh, A., and Lawson, W.: Franz Josef and Fox Glaciers, New Zealand: Historic length records, Global and Planetary Change, 121, 41–52, https://doi.org/https://doi.org/10.1016/j.gloplacha.2014.06.008, 2014.

Roe, G. H. and Baker, M. B.: Glacier response to climate perturbations: An accurate linear geometric model, Journal of Glaciology, 60, 670–684, https://doi.org/10.3189/2014JoG14J016, 2014.

Roe, G. H. and O'Neal, M. A.: The response of glaciers to intrinsic climate variability: Observations and models of late-holocene variations in the Pacific northwest, Journal of Glaciology, 55, 839–854, https://doi.org/10.3189/002214309790152438, 2009.

Schaefer, J. M., Denton, G. H., Kaplan, M., Putnam, A., Finkel, R. C., Barrell, D. J., Andersen, B. G., Schwartz, R., Mackintosh, A., Chinn, T., and Schlüchter, C.: High-frequency holocene glacier fluctuations in new zealand differ from the northern signature, Science, 324, 622–625, https://doi.org/10.1126/science.1169312, 2009.

Schmidt, G. A., Jungclaus, J. H., Ammann, C. M., Bard, E., Braconnot, P., Crowley, T. J., Delaygue, G., Joos, F., Krivova, N. A., Muscheler, R., Otto-Bliesner, B. L., Pongratz, J., Shindell, D. T., Solanki, S. K., Steinhilber, F., and Vieira, L. E. A.: Climate forcing reconstructions for use in PMIP simulations of the last millennium (v1.0), Geoscientific Model Development, 4, 33–45, https://doi.org/10.5194/gmd-4-33-2011, 2011.

Solomina, O. N., Bradley, R. S., Hodgson, D. A., Ivy-Ochs, S., Jomelli, V., Mackintosh, A. N., Nesje, A., Owen, L. A., Wanner, H., Wiles, G. C., and Young, N. E.: Holocene glacier fluctuations, Quaternary Science Reviews, 111, 9–34, https://doi.org/10.1016/j.quascirev.2014.11.018, http://dx.doi.org/10.1016/j.quascirev.2014.11.018, 2015.

Stenchikov, G., Delworth, T. L., Ramaswamy, V., Stouffer, R. J., Wittenberg, A., and Zeng, F.: Volcanic signals in oceans, Journal of Geophysical Research: Atmospheres, 114, D16 104, https://doi.org/10.1029/2008JD011673, 2009.

Wallace, J. M. and Hobbs, P. V.: Atmospheric Science: An Introductory Survey, Academic Press, 2006.

Young, J., Pettit, E. C., Arendt, A. A., Hood, E., Liston, G., and Beamer, J. P.: A changing hydrological regime: Trends in magnitude and timing of glacier ice melt and glacier runoff in a high latitude coastal watershed, Earth and Space Science Open Archive, p. 61, https://doi.org/10.1002/essoar.10502440.1, https://doi.org/10.1002/essoar.10502440.1, 2020.

https://doi.org/10.5194/tc-2020-230
Preprint. Discussion started: 28 August 2020

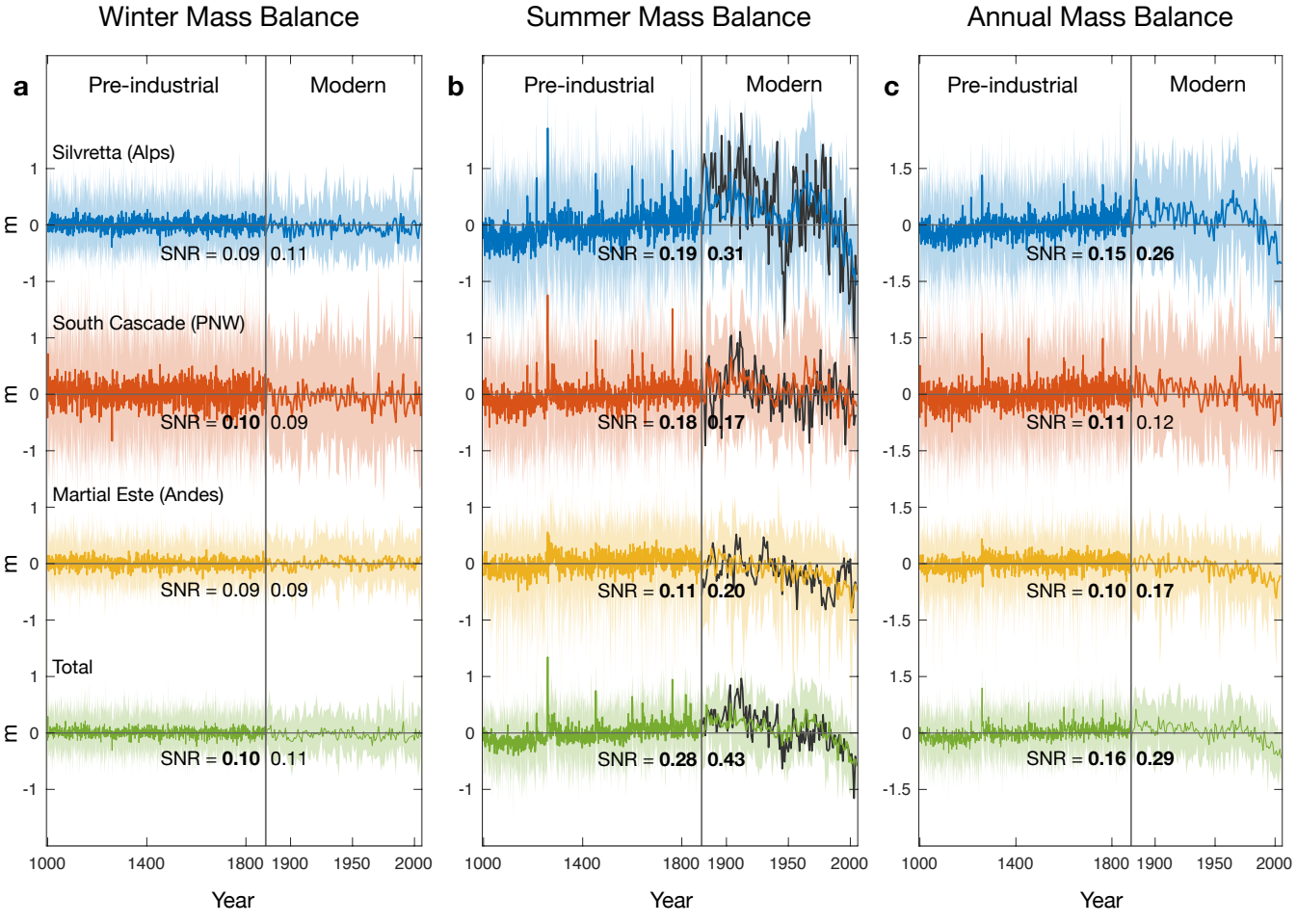

Figure 1. Anomalies of (a) winter mass balance, (b) summer mass balance, and (c) annual mass balance within the LME at locations near representative glaciers in the Alps (blue), the Pacific Northwest (red), and the Patagonian Andes (yellow), along with their results when averaged together (green). Heavy colors represent the ensemble mean, while lighter colors represent individual ensemble members. The vertical grey line at the year 1880 marks the approximate transition from the pre-industrial era to the modern era, after which the time axis on each panel is dilated by a factor of 4 to enhance visibility. To evaluate the accuracy of LME temperatures over the modern era, we also plot values of b'_s calculated from the observational NASA-GISS surface temperature data set in black. SNR values are given for each glacier and era, with bold font indicating statistical significance (99% confidence; see Appendix).

https://doi.org/10.5194/tc-2020-230
Preprint. Discussion started: 28 August 2020

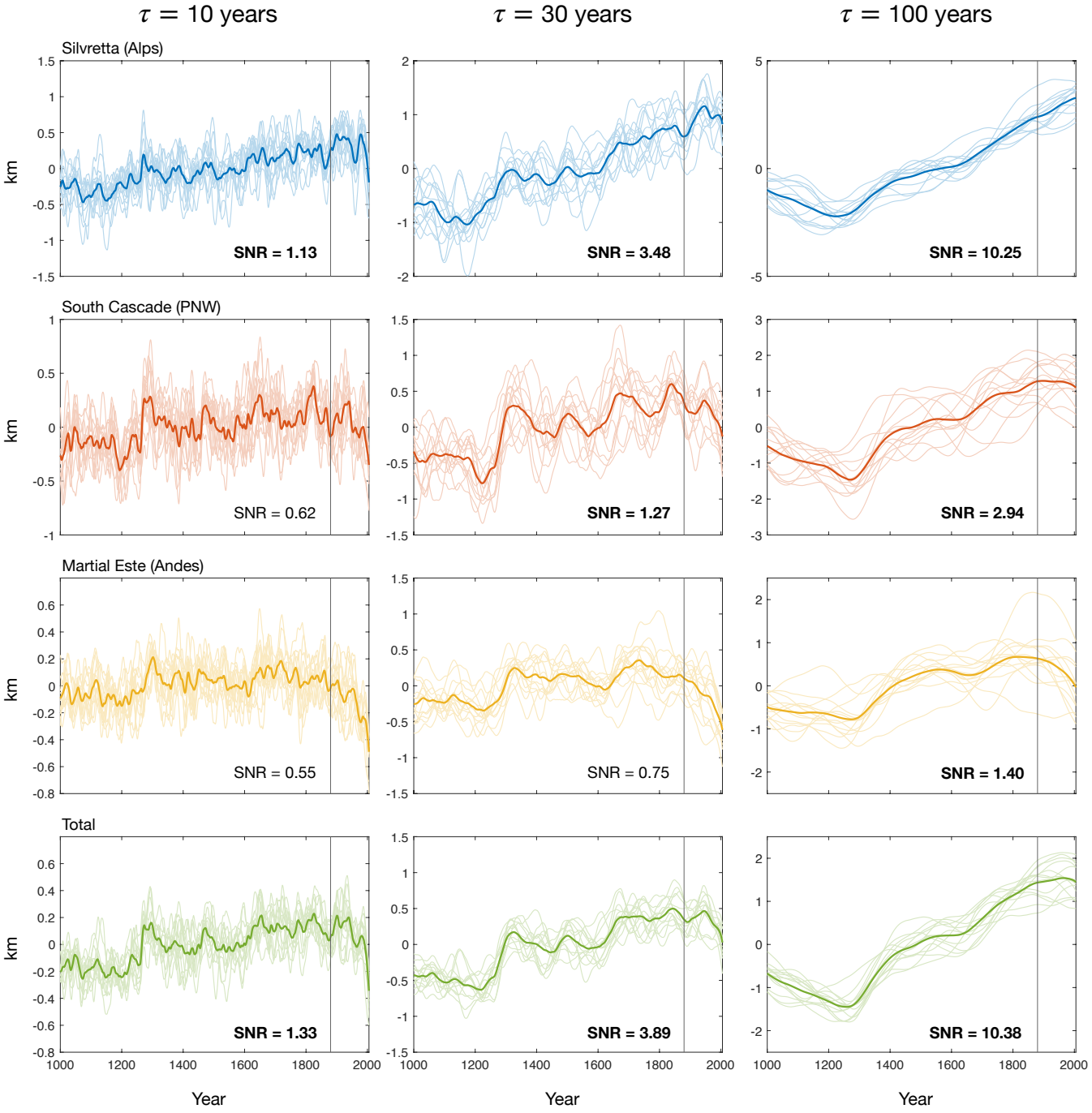

Figure 2. Simulated glacier length anomalies for representative glaciers in the Alps (top row), the Pacific Northwest (second row), and the Patagonian Andes (third row). The fourth row shows the sum of all three glaciers. Columns indicate response timescales of $\tau = 10$ years (left), $\tau = 30$ years (middle), and $\tau = 100$ years (right). Heavy colors represent the ensemble mean, while shaded colors represent individual ensemble members. The vertical grey line at the year 1880 marks the transition from the pre-industrial era to the modern era. SNR values are computed over the pre-industrial era only. Bold font indicates $\mathrm{SNR} > 1$, meaning that the forced signal exceeds the noise of internal variability.

https://doi.org/10.5194/tc-2020-230
Preprint. Discussion started: 28 August 2020

The Cryosphere
Discussions
Open Access
EGU

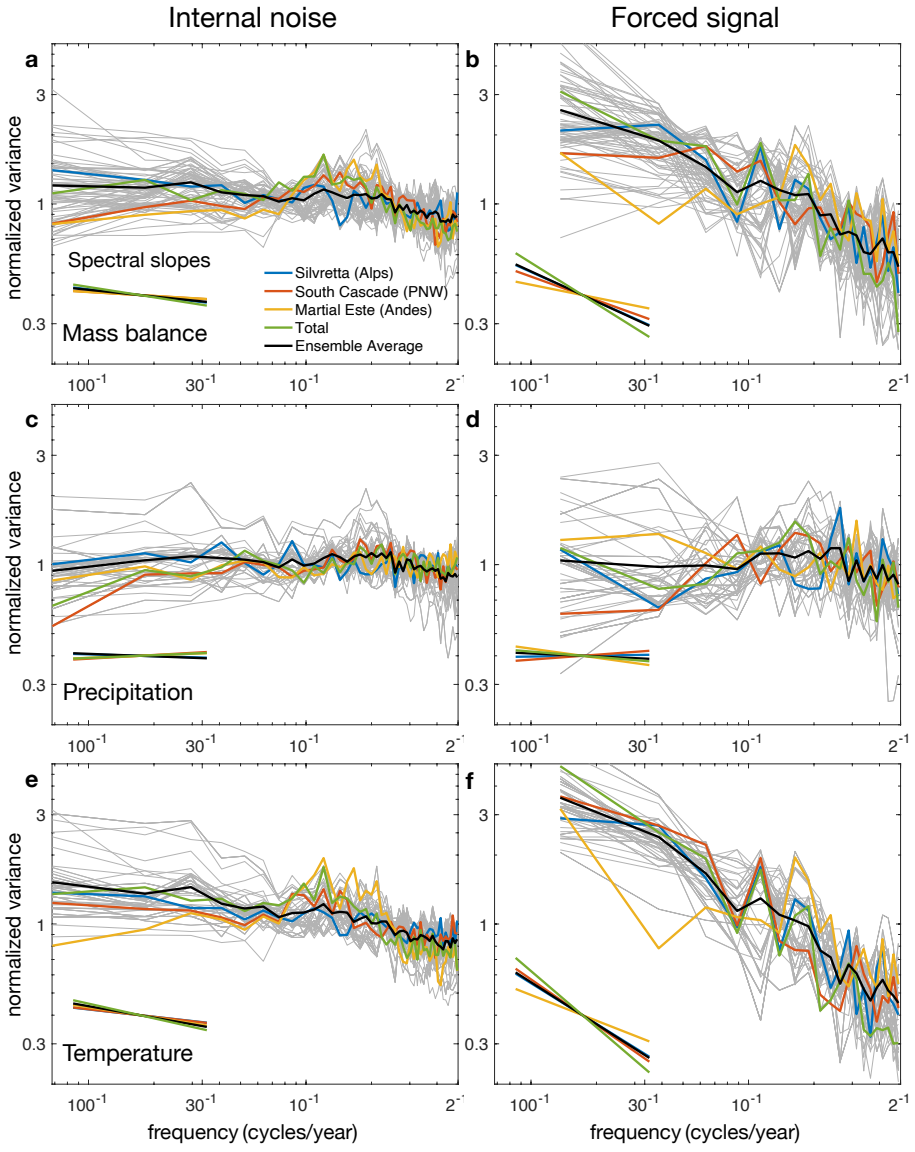

Figure 3. Frequency spectra of unforced (left column) and forced (right column) variability in annual mass balance (top row), winter precipitation (middle row), and summer temperature (bottom row). Spectra are shown for Silvretta (blue), South Cascade (red), Martial Este (yellow), and the other 73 glaciers (gray). The green line shows the spectrum of the average time series among the three glaciers. The black line shows the average of all 76 individual spectra. Lines in the bottom left of each panel show the slope of the least-squares regression line for each spectrum. Spectra were computed using periodograms with a Hanning window equal to one-third the length of the data. Unforced spectra were averaged among the 13 ensemble members. Forced spectra were band-averaged to reduce noise, explaining the coarser spectral resolution.

https://doi.org/10.5194/tc-2020-230
Preprint. Discussion started: 28 August 2020

The Cryosphere
Discussions
Open Access
EGU

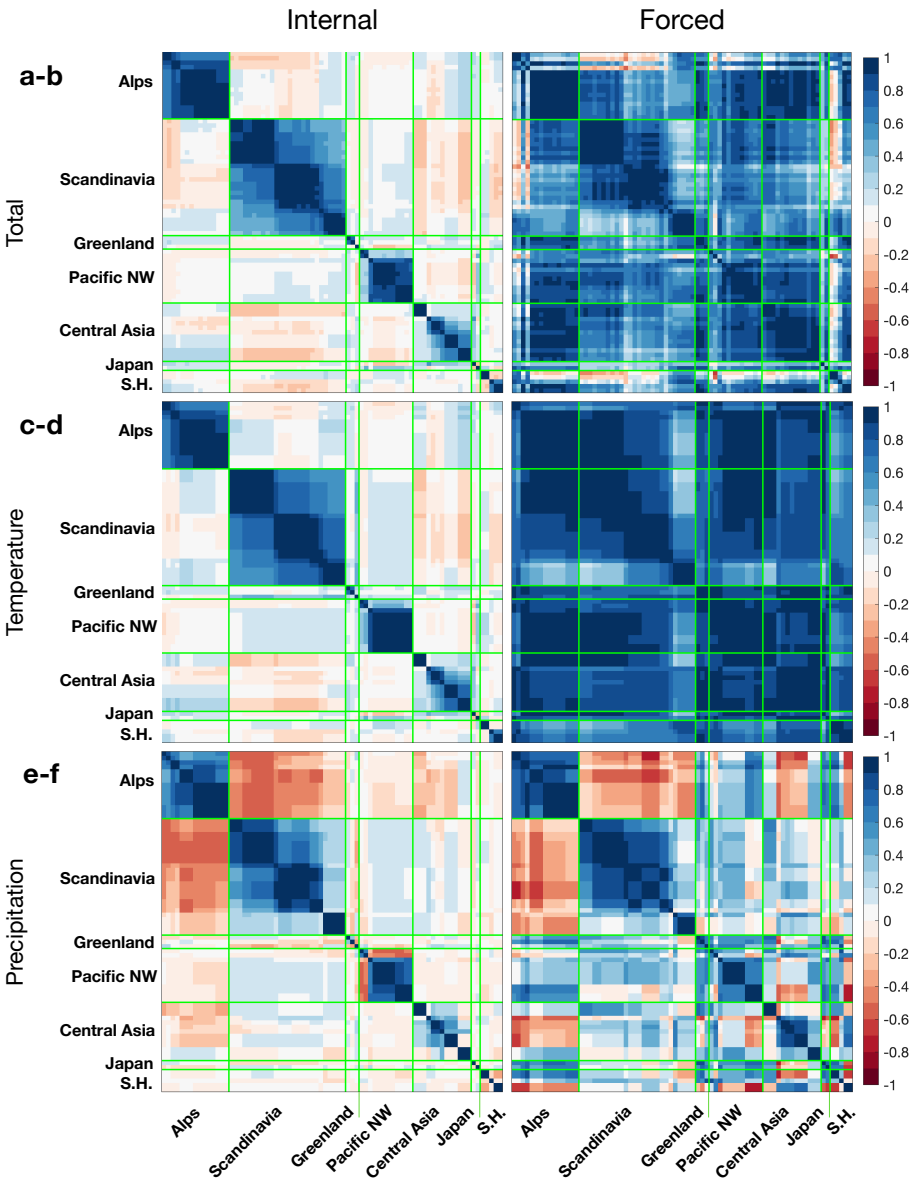

Figure 4. Cross-correlation matrices of glacier length variability driven by internal (left column) and forced (right column) climate variability over the last millennium (1000-1999 CE). (a-c) Total variability from both summer temperature and winter precipitation. (c-d) Variability from summer temperature. (e-f) Variability from winter precipitation. Glaciers are grouped into 7 regions divided by green lines: the Alps (including the Pyrenees), Scandinavia, Greenland, the Pacific Northwest/Alaska, Central Asia, Japan, and the Southern Hemisphere. Blue (red) colors indicate positive (negative) correlations between glaciers on the x- and y-axes.

https://doi.org/10.5194/tc-2020-230
Preprint. Discussion started: 28 August 2020

The Cryosphere
Discussions
Open Access
EGU

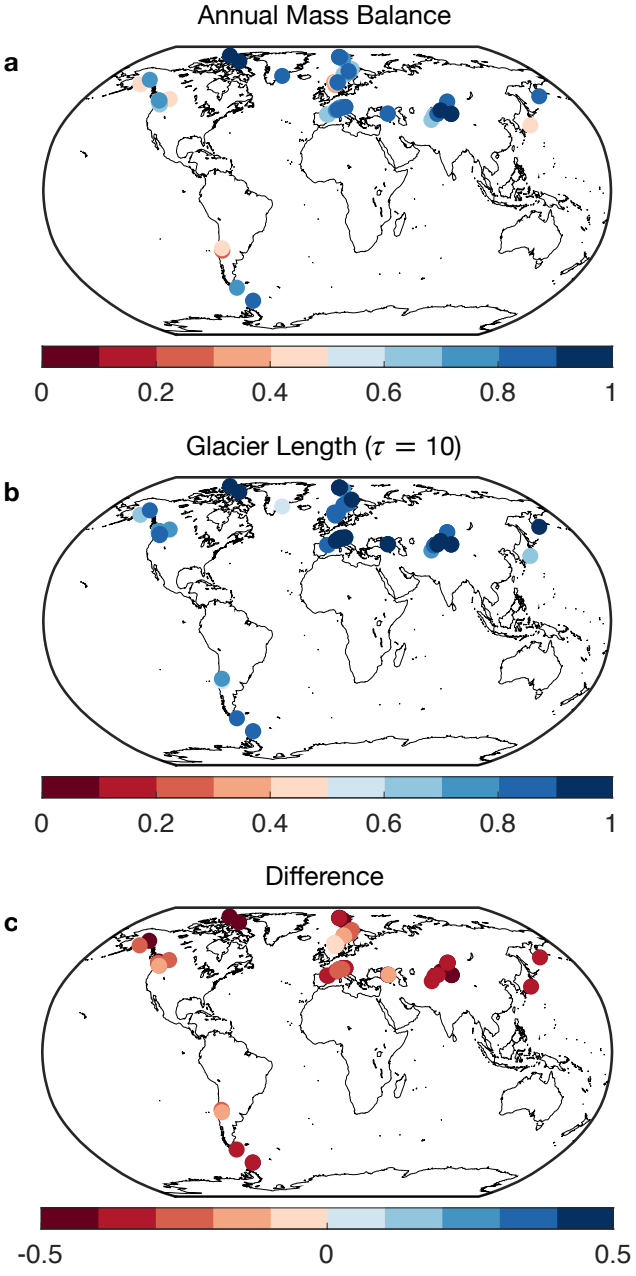

Figure 5. The fraction of total variance in (a) annual mass balance and (b) glacier length ($\tau = 10$ years) due to variance in summer temperature. The remaining variance is due to winter precipitation. (c) The difference between (b) and (a); positive values indicate that summer temperature accounts for a larger fraction of variance in glacier length than in annual mass balance.

https://doi.org/10.5194/tc-2020-230
Preprint. Discussion started: 28 August 2020

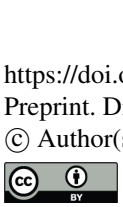

The Cryosphere
Discussions
Open Access
EGU

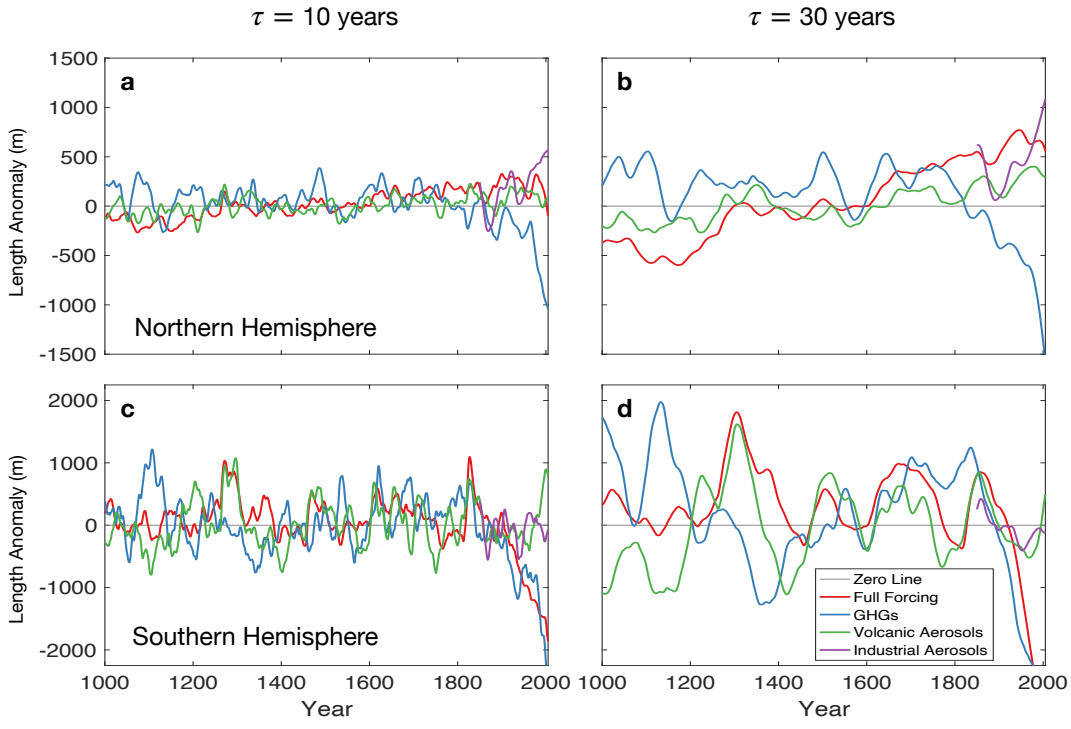

Figure 6. Contributions of individual forcings to glacier length variability over the last millennium for response timescales of $\tau = 10$ years (left column) and $\tau = 30$ years (right column). (a-b) The average of all Northern Hemisphere glaciers. (c-d) The average of all Southern Hemisphere glaciers. Colors represent the contributions from individual forcings, which we approximate from the ensemble-mean time series of summer temperature and winter precipitation within each single-forcing ensemble. The individual forcings are greenhouses gases (blue), volcanic aerosols (green), and industrial aerosols (purple). The red line shows the combined influence of all forcings diagnosed from the full 13-member ensemble.

https://doi.org/10.5194/tc-2020-230
Preprint. Discussion started: 28 August 2020

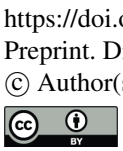

The Cryosphere
Discussions
Open Access
EGU

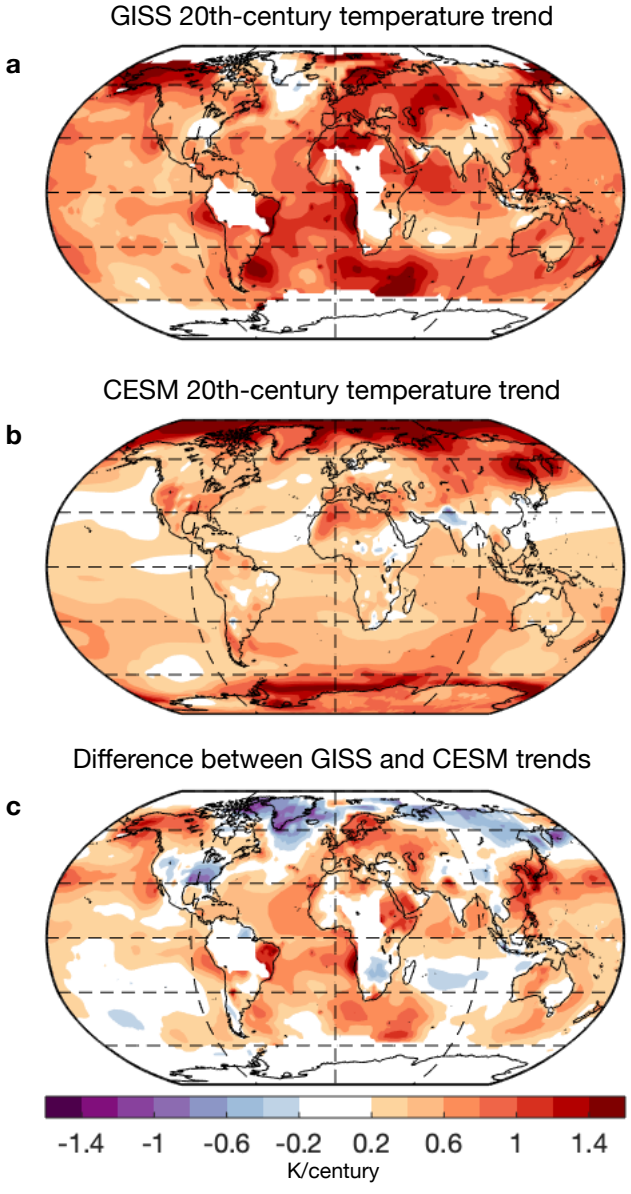

Figure A1. Linear trend in 2-m air temperature (in units of K/century) between 1900-1999 in (a) the NASA GISS observational dataset and (b) the CESM LME ensemble mean. (c) The difference between (a) and (b). Warmer temperatures are shown in red, with cooler temperatures shown in blue.

https://doi.org/10.5194/tc-2020-230
Preprint. Discussion started: 28 August 2020

The Cryosphere Discussions
Open Access
EGU

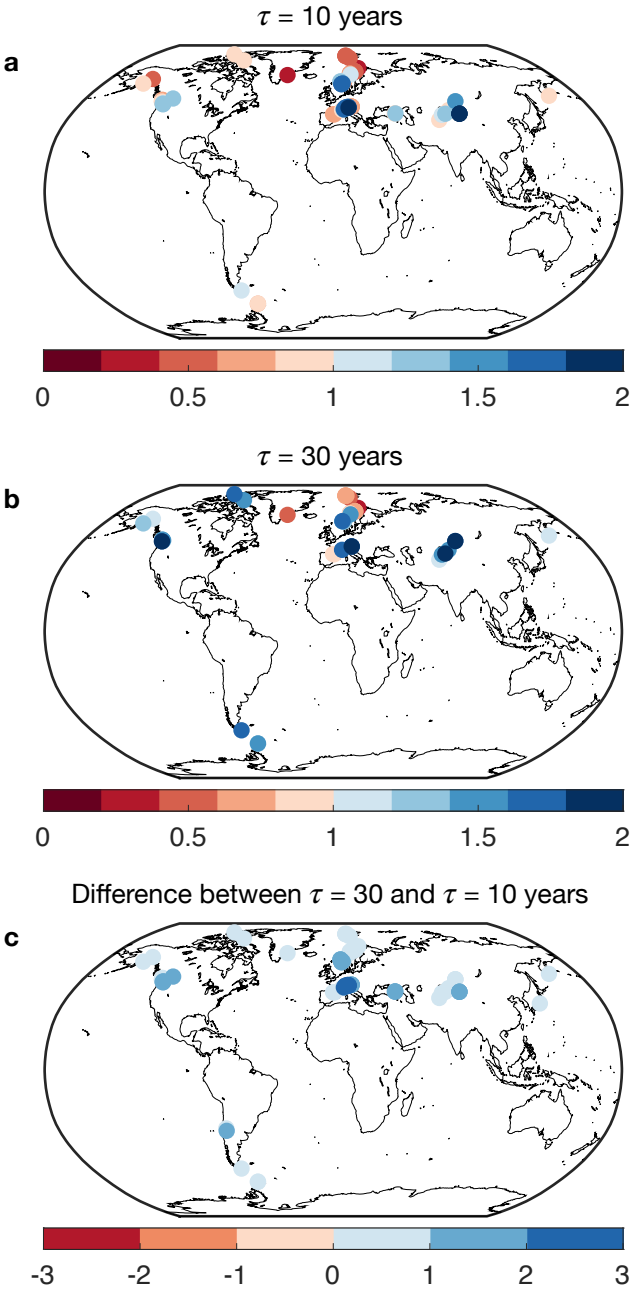

Figure A2. The signal-to-noise ratio (SNR) for all 76 glacier locations given (a) $\tau = 10$ years and (b) $\tau = 30$ years. (c) The difference between (b) and (a). Red colors in (a) and (b) indicate a larger role for internal variability than forced variability, while blue colors indicate the opposite. Blue colors in (c) indicate a greater role for forced variability when $\tau = 30$ years than when $\tau = 10$ years.

https://doi.org/10.5194/tc-2020-230
Preprint. Discussion started: 28 August 2020

The Cryosphere
Discussions
Open Access
EGU

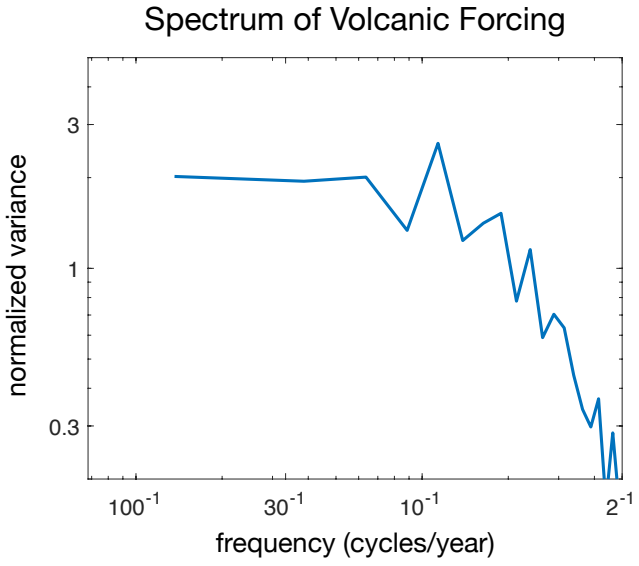

Figure A3. Frequency spectra of volcanic forcing generated from time series of volcanic aerosol concentrations in the LME (courtesy of John Fasullo).

https://doi.org/10.5194/tc-2020-230
Preprint. Discussion started: 28 August 2020

The Cryosphere Discussions
Open Access
EGU

Table A1. Glacier data from Medwedeff and Roe (2017). Glaciers are excluded if observations of summer or winter mass balance span less than 10 years. $\sigma_{b,w}$: the standard deviation of observed winter mass balance (in m). $\sigma_{b,s}$: the standard deviation of observed summer mass balance (in m). σ_P: the standard deviation of simulated winter precipitation within the LME over the last millennium (1000-1999) (in m). σ_T: the standard deviation of simulated summer temperature within the LME over the last millennium (1000-1999) (in K). α: the ratio of $\sigma_{b,w}/\sigma_P$. λ: the ratio of $\sigma_{b,s}/\sigma_T$ (in m K^{-1}).

Glacier	Lat	Lon	$\sigma_{b,w}$	$\sigma_{b,s}$	σ_P	σ_T	α	λ
SARENNES	45.13	6.13	0.51	0.85	0.07	0.72	7.03	1.17
STORBREEN	61.57	8.13	0.38	0.47	0.16	0.84	2.39	0.56
DEVON ICE CAP NW	75.42	-83.25	0.02	0.16	0.02	1.32	1.30	0.12
SILVRETTA	46.85	10.08	0.34	0.67	0.09	0.60	3.86	1.11
SOUTH CASCADE	48.37	-121.05	0.65	0.58	0.16	0.68	4.18	0.85
HELLSTUGUBREEN	61.56	8.44	0.27	0.50	0.16	0.84	1.73	0.60
NIGARDSBREEN	61.72	7.13	0.61	0.59	0.16	0.84	3.88	0.70
GRAASUBREEN	61.65	8.60	0.25	0.51	0.16	0.84	1.56	0.60
GRIES	46.44	8.33	0.39	0.63	0.09	0.60	4.20	1.04
VERNAGT FERNER	46.88	10.82	0.22	0.42	0.09	0.60	2.52	0.70
AALFOTBREEN	61.75	5.65	1.07	0.73	0.19	0.67	5.76	1.08
GULKANA	63.25	-145.42	0.29	0.51	0.05	1.06	6.52	0.48
WOLVERINE	60.40	-148.92	0.80	0.65	0.12	1.04	6.91	0.63
DJANKUAT	43.20	42.77	0.41	0.46	0.07	0.74	5.93	0.62
STORGLACIAEREN	67.90	18.57	0.38	0.49	0.06	1.08	6.00	0.45
REMBESDALSKAAKA	60.53	7.36	0.75	0.54	0.14	0.71	5.27	0.76
ENGABREEN	66.65	13.85	0.78	0.71	0.12	1.00	6.21	0.70
HAMAGURI YUKI	36.60	137.62	1.63	1.52	0.08	0.70	19.69	2.18
TS.TUYUKSUYSKIY	43.05	77.08	0.21	0.44	0.03	0.65	7.94	0.68
ECHAURREN NORTE	-33.57	-70.13	1.24	0.71	0.13	0.63	9.71	1.12
WURTEN K.	47.03	13.00	0.29	0.57	0.09	0.64	3.24	0.89
GARABASHI	43.30	42.47	0.17	0.41	0.07	0.74	2.48	0.56
PEYTO	51.67	-116.53	0.40	0.38	0.05	0.73	7.83	0.53
AUSTRE BROEGGERBREEN	78.88	11.83	0.12	0.30	0.05	1.48	2.36	0.20
FONTANA BIANCA / WEISSBRUNNF.	46.48	10.77	0.38	0.61	0.09	0.60	4.30	1.01
MIDTRE LOVENBREEN	78.88	12.07	0.13	0.29	0.05	1.48	2.65	0.20
MALIY AKTRU	50.08	87.75	0.27	0.30	0.05	0.69	5.76	0.43
PLACE	50.43	-122.60	0.31	0.47	0.19	0.88	1.60	0.54
SHUMSKIY	45.08	80.23	0.08	0.42	0.03	0.74	2.78	0.57
PILOTO ESTE	-32.22	-70.05	0.58	0.55	0.13	0.63	4.58	0.87

https://doi.org/10.5194/tc-2020-230
Preprint. Discussion started: 28 August 2020

Table A1. Continued.

Glacier	Lat	Lon	$\sigma_{b,w}$	$\sigma_{b,s}$	σ_P	σ_T	α	λ
SENTINEL	49.90	-122.98	0.67	0.47	0.19	0.88	3.43	0.54
AUSTDALSBREEN	61.81	7.35	0.65	0.62	0.16	0.84	4.10	0.74
RIUKOJIETNA	68.08	18.08	0.39	0.59	0.06	1.08	6.17	0.54
MARMAGLACIAEREN	68.83	18.67	0.21	0.46	0.09	1.03	2.36	0.44
HANSEBREEN	61.75	5.68	0.92	0.75	0.19	0.67	4.95	1.11
LANGFJORDJOEKULEN	70.12	21.73	0.36	0.52	0.06	1.11	5.70	0.47
RABOTS GLACIAER	67.91	18.50	0.38	0.47	0.06	1.08	6.13	0.44
HANSBREEN	77.08	15.67	0.17	0.29	0.07	1.70	2.33	0.17
MALADETA	42.65	0.63	0.51	0.64	0.06	0.81	7.99	0.79
CIARDONEY	45.51	7.39	0.49	1.29	0.09	0.60	5.25	2.15
TARFALAGLACIAEREN	67.93	18.65	0.44	0.74	0.06	1.08	7.01	0.68
VODOPADNIY (NO.125)	50.10	87.70	0.10	0.22	0.05	0.69	2.09	0.32
JAMTAL F.	46.87	10.17	0.25	0.49	0.09	0.60	2.88	0.81
KOZELSKIY	53.23	158.82	0.61	1.22	0.09	1.05	6.84	1.16
KONGSVEGEN	78.80	12.98	0.15	0.31	0.05	1.48	3.03	0.21
BASODINO	46.42	8.48	0.48	0.62	0.09	0.60	5.19	1.03
URUMQI GLACIER NO. 1 W-BRANCH	43.08	86.82	0.09	0.44	0.01	0.58	15.08	0.76
GRAAFJELLSBREA	60.08	6.39	0.73	0.60	0.14	0.71	5.12	0.84
GOLUBIN	42.46	74.49	0.15	0.23	0.04	0.72	3.74	0.32
LEVIY AKTRU	50.08	87.72	0.15	0.24	0.05	0.69	3.16	0.35
URUMQI GLACIER NO. 1	43.08	86.82	0.09	0.33	0.01	0.58	15.46	0.57
BREIDABLIKKBREA	60.07	6.36	0.80	0.55	0.14	0.71	5.58	0.78
HELM	49.97	-123.00	0.41	0.56	0.19	0.88	2.11	0.64
TBILISA	43.13	42.47	0.14	0.31	0.07	0.74	2.05	0.43
ABRAMOV	39.63	71.6	0.32	0.41	0.08	0.93	4.02	0.44
MEIGHEN ICE CAP	79.95	-99.13	0.03	0.28	0.02	1.13	1.93	0.25
CARESER	46.45	10.70	0.38	0.44	0.09	0.60	4.28	0.74
KLEINFLEISS K.	47.05	12.95	0.26	0.54	0.09	0.64	2.90	0.85
GOLDBERG K.	47.04	12.97	0.25	0.56	0.09	0.64	2.72	0.88
URUMQI GLACIER NO. 1 E-BRANCH	43.08	86.82	0.06	0.36	0.01	0.58	10.18	0.62
MITTIVAKKAT	65.67	-37.83	0.14	0.37	0.21	1.27	0.69	0.29
NORTH KLAWATTI	48.57	-121.12	0.91	1.15	0.16	0.68	5.83	1.69
SILVER	48.98	-121.25	0.72	0.98	0.19	0.68	3.80	1.44
NOISY CREEK	48.67	-121.53	0.99	1.13	0.19	0.68	5.22	1.66

https://doi.org/10.5194/tc-2020-230
Preprint. Discussion started: 28 August 2020

Table A1. Continued.

Glacier	Lat	Lon	$\sigma_{b,w}$	$\sigma_{b,s}$	σ_P	σ_T	α	λ
MARTIAL ESTE	-54.78	-68.40	0.28	0.49	0.04	0.49	7.10	1.00
OSSOUE	42.77	-0.14	0.54	0.78	0.07	0.69	7.49	1.14
ZAVISHA	50.80	-123.42	0.31	0.51	0.19	0.88	1.60	0.58
SYKORA	50.87	-123.58	0.27	0.54	0.19	0.88	1.40	0.62
STORGLOMBREEN	66.67	14.00	0.50	0.72	0.12	1.00	3.97	0.72
TROLLBERGDALSBREEN	66.71	14.44	0.53	0.57	0.12	1.00	4.21	0.57
OKSTINDBREEN	66.01	14.29	0.69	0.51	0.08	1.01	8.75	0.50
GRAND ETRET	45.47	7.21	0.58	0.47	0.09	0.76	6.55	0.61
STORSTEINSFJELLBREEN	68.22	17.92	0.35	0.29	0.09	1.03	3.96	0.28
WALDEMARBREEN	78.67	12.00	0.13	0.17	0.05	1.48	2.66	0.11
JOHNSONS	-62.66	-60.35	0.17	0.22	0.05	0.99	3.38	0.22
HURD	-62.68	-60.40	0.14	0.30	0.05	0.99	2.72	0.31